

Experimental and Numerical Investigation of the Oscillation of an Inverted Flag

Samson Annapureddy

Department of Mechanical,
Materials and Aerospace Engineering
Illinois Institute of Technology
Chicago, IL, 60616
sannapureddy@iit.edu

Anvar Gilmanov

Saint Anthony Falls Laboratory.
University of Minnesota
Minneapolis, MN, 55414
agilmano@umn.edu

Sumanta Acharya

Department of Mechanical,
Materials and Aerospace Engineering
Illinois Institute of Technology
Chicago, IL, 60616
sacharya1@iit.edu

Henryk Stolarski

Civil Environmental and Geo-Engineering ...
University of Minnesota
Minneapolis, MN, 55414
stola001@umn.edu

ABSTRACT

In this paper, we investigate the oscillations of an inverted flag using both experiments and computations. The term "inverted flag" refers to a cantilever-type sheet submerged in a fluid flowing from its free edge towards the fixed end. The flag-oscillations are controlled by the interaction between the destabilizing flow instabilities and the stabilizing structural stiffness. Recent studies (Kim et al. 2013) have demonstrated strong large-amplitude self-sustained oscillations of the flag that can potentially be exploited for beneficial purposes such as harvesting energy. Experiments are carried out in an open-loop wind tunnel and instantaneous velocities are measured with Planar Particle Image Velocimetry (PIV). The corresponding numerical simulations are undertaken using a recently-developed CURVIB-FE-FSI approach to simulate fluid-structure interaction with strong nonlinear deformation of thin structures (Gilmanov et al. 2015). The experimental results and computations are in good agreement. Phase averaged analyses reveal that the inverted flag undergoes oscillations due to vortex induced vibration and exhibit a periodic motion that results in large-amplitude flapping over a finite band of free-stream velocities. At higher velocities, the flag exhibits a fully-deflected mode, which is in agreement with the observations of Kim et al. (2013). The flow and structure interactions are governed by growth and breakdown of large-scale structures at the leading-edge of the flag. The turbulent fluctuations are a maximum in the vicinity of the leading edge during the forward motion of the flag, and the fluctuations dissipate as the flag retracts.

Keywords: Inverted flag, Vortex induced vibrations(VIV), Flow and structure interactions.

NOMENCLATURE

Re	[-]	Reynolds Number based on length of the flag
U	[m/s]	Free-stream velocity
u	[m/s]	Streamwise component of velocity
v	[m/s]	Wall normal component of velocity

L	[mm]	Length of the flag
H	[mm]	Width of the flag
h	[mm]	Thickness of the flag
ρ	[kg/m ³]	Density
x	[mm]	Streamwise coordinate
y	[mm]	Normal coordinate
z	[mm]	Spanwise coordinate
f	[Hz]	Frequency of flag oscillations
β	[-]	Bending stiffness
μ	[-]	Mass ratio

Subscripts

s	Solid
f	Fluid

INTRODUCTION

A cantilevered flexible sheet immersed in a uniform flow undergoes self-induced and self-sustained oscillations due to fluid-structure interactions (FSI). In the past, extensive studies (e.g., Alben and Shelley 2008; Argentina and Mahadevan 2005; Michelin et al. 2008, Eloy et al. 2007 and 2008, Connell and Yue 2007 and Zhu and Peskin 2002) have been carried out to understand the dynamics of a cantilevered sheet, where the flow is from the clamped leading-edge to the free trailing edge (termed as conventional flag). Applications for the conventional flag configuration span from paper printing (Watanabe et al. 2002 a, b), flow control devices (Lucey 1998; Jaiman, Loth & Dutton 2004), botanical applications (Huang, Rominger & Nepf 2011), and energy harvesting (Allen and Smits 2001; Tang et al. 2009 and Michelin and Doare 2013).

In recent years, investigations have been directed at the "inverted flag" configuration where the flow direction is from the free-end to the cantilevered-end of the flag. To investigate the effects of flow orientation, experiments were carried out by Rinaldi and Paidoussis (2012) on a cantilevered slender cylindrical rod. The authors observed that the rod exhibits small-amplitude flutter oscillations (amplitude less than the cylinder diameter) occurring at low flow speeds which gives way to an abrupt deflected

equilibrium at higher speeds due to a static divergence. For an inverted flag, Kim et al. (2013), showed that the parameter that governs the dynamics of the flow-structure-interaction (FSI) problem is the non-dimensional bending stiffness (β) and identified three regimes of flag response as a function of β : (1) the straight mode, where the flag is too rigid to be deflected by the flow and remains straight (large values of β); (2) the flapping mode, where the flag undergoes large amplitude flapping oscillations (intermediate values of β); and (3) the deflected mode, where the flag is so flexible that it is deflected by the flow toward one side and remains fixed at this position at all times (small β values). Following the work of Kim et al. (2013), Direct Numerical Simulations (DNS) of Gurugubelli and Jaiman (2015) on the oscillations of flexible foil at low Re and a detailed theoretical and experimental work of Sader et al. (2016) in the range of Re $O(10^4)$ - (10^5) for varying aspect ratio and fluid loading suggests that the flapping is initiated immediately following the divergence instability. Further, using scaling analysis, Sader et al. (2016) provided evidence that flapping occurs because of vortex induced vibrations. They also observed that periodic vortex shedding from the leading edge of the flag is synchronized with flapping motion of the flag. The DNS studies of Ryu et al. (2015) and Tang et al. (2015), at low Re , were also successful in reproducing the experimentally observed phenomenon.

In this paper, we have undertaken experiments and computations for the inverted flag, and report phase-averaged velocity and turbulence field measurements complemented by instantaneous velocity fields from the computations. The goal of the combined experimental-computational study is to improve the understanding of the FSI flow physics for the inverted-flag, besides investigating the hypothesis that the inverted flag oscillations are a result of vortex induced vibrations (VIV) which is not fully explored in the literature. Experiments are primarily carried out using Particle Image Velocimetry while computations are undertaken using Finite-Elements (FE) for the structure, Large Eddy Simulations (LES) for the flowfield and an Immersed Boundary (IB) approach in the FSI calculations (Gimlanov et al., 2015).

EXPERIMENTAL AND COMPUTATIONAL DETAILS

Measurements are carried out in an open-loop wind tunnel having a test section cross-section of 380mm×380mm. The flag is realized from a polycarbonate sheet of thickness $h = 0.254$ mm, while the length (L) and width (H) of the flag are 100mm (Poisson's ratio $\nu = 0.38$, Young's modulus $E = 2.38 \times 10^9$ N/m² and density $\rho_s = 1.2 \times 10^3$ kg/m³). Reynolds number, based on the inflow velocity and flag length, is 32428. A circular cylinder of 8mm diameter is used to clamp the downstream end of the sheet. The flag is held parallel to the flow by fixing the aluminium cylinder to the side walls of the tunnel, Fig.1. A small tip deflection $0.01 < (\Delta/L) < 0.03$ is found in the initial sheet configuration. Flexural rigidity, bending stiffness (β) and mass ratio (μ) are defined following the work of Kim et al. (2013) and the values of bending stiffness is varied in the range of 0.35 to 0.06, while the mass ratio is 2.54.

Flag motion is captured using a 256×256 pixel high-speed camera (Kodak, Ekta-Pro). Images are recorder at 1125 frames per

second and the deflection of the sheet is calculated by tracking the flag-leading.

Instantaneous velocity field is measured from Planar Particle Image Velocimetry (PIV). The flow is seeded with one micron diameter particles produced by Rosco mini-V, while the measuring plane is illuminated by a laser sheet at 532nm emitting from a set of two Nd:Yag Quantel Evergreen laser cavities of 200 mJ/pulse each, with a repetition rate of 15Hz. A 29MP CCD camera is used for acquiring images. The time delay between the laser cavities and image-pair acquisition is controlled from a delay generator connected to a workstation. The time delay is calculated based on the free-stream velocity considering the particle displacement in an image pair equivalent to 10–15% of interrogation window size. The measurement uncertainty level for the velocity vectors, and Reynolds stress $\langle u'v' \rangle$, is estimated to be within 2% and 5% respectively. The uncertainty level of the spanwise vorticity data is expected to be within 10.0%.

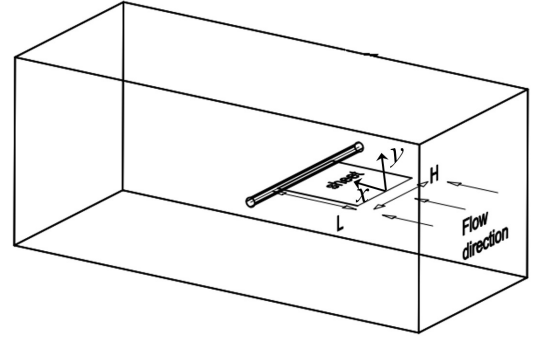


Figure: 1 Schematic of the experimental setup.

Phase averaged analyses is realized from “Bin-averaging” technique, where data is collected in bins. Since the flag oscillates about its mean position, each time period (τ_0) is subdivided into smaller intervals, which will be referred to as bins. Groups of neighbouring bins are called intervals. The center of each bin and each interval is marked by a phase angle (θ) which assumes values in the range of 0 to 90. Thus, phase averages are computed from all velocity samples which were collected at the same bin. The mean and the root mean square value of velocity components are calculated using equations (1) and (2).

$$U(\theta) = \frac{1}{N(\theta)} \sum_{n=1}^{N(\theta)} u_n(\theta) \quad (1)$$

$$u_{rmsB}(\theta) = \sqrt{\frac{1}{N(\theta)-1} \sum_{n=1}^{N(\theta)} (u_n(\theta) - U(\theta))^2} \quad (2)$$

Computations are provided by using a new numerical methodology CURVIB-FE-FSI for simulating FSI problems involving thin flexible bodies in an incompressible fluid. The FSI algorithm uses the Dirichlet–Neumann partitioning technique. The curvilinear immersed boundary method (CURVIB) is coupled with a rotation-free finite element (FE) model for thin shells (Stolarski, et al. 2013) enabling the efficient simulation of FSI problems with arbitrarily large deformation (Gimlanov et al. 2015). Turbulent

flow problems are handled using LES with the dynamic Smagorinsky model in conjunction with a wall model to reconstruct boundary conditions near immersed boundaries (Kang et al. 2011).

The coupled CURVIB-FE-FSI method is validated by applying it to simulate two FSI problems involving thin flexible structures: 1) vortex-induced vibrations of a cantilever mounted in the wake of a square cylinder at different mass ratios and at low Reynolds number; and 2) the more challenging high Reynolds number problem involving the oscillation of an inverted elastic flag. For both cases the computed results are in excellent agreement with previous numerical simulations and/or experimental measurements (Gilmanov et al. 2015). Grid convergence tests are carried out for both the cantilever and inverted flag problems, which show that the CURVIB-FE-FSI method provides their convergence.

The simulations have been performed for the same values of the various governing parameters as it was described above. The corresponding Reynolds number, based on the inflow velocity and flag length, is $Re = u_\infty L \rho_f / \mu = 99505$, and, therefore, the massively separated flow in the wake of the flapping flag is expected to be turbulent. To capture that CURVIB-FE-FSI method in LES mode has been employed. The plate surface is discretized with 206 triangular elements and the background fluid grid is discretized with a uniform Cartesian mesh with $561 \times 201 \times 201$ in the streamwise (x), vertical (y) and transverse (z) directions, respectively.

RESULTS AND DISCUSSIONS

In this section, experimental and computational results are presented to elucidate the dynamics of an inverted flag for $\beta=0.13$. The tip of the flag is considered as origin. Inverted flag in the following text is termed simply as the flag.

Characteristics of the flag

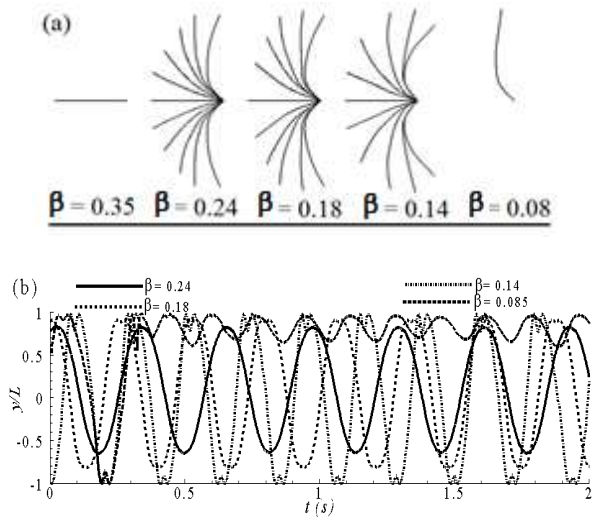


Figure: 2 Evolution of flag oscillations from stable equilibrium to deflected mode: (a) Schematic from high-speed camera measurements and (b) time history of tip trajectory.

Figure 2(a), shows the schematic of evolution of flag oscillations for increasing velocity (decreasing β) following the present experiments. It is observed that for larger values of bending stiffness ($\beta > 0.25$) the flag remained in stable equilibrium state. As β decreases the flag suddenly undergoes periodic oscillation in the range of $0.24 \leq \beta \leq 0.1$, following static divergence instability (Sader et al 2016). Further, a local maximum and minimum in the vicinity of flag tip's extreme position is observed for $0.14 \leq \beta \leq 0.1$. For $\beta < 0.1$ the flag remains in a deflected mode. The corresponding tip trajectories from high-speed camera measurements are shown in Fig.2(b).

Normalised tip trajectories w.r.t flapping period obtained from experiments and computations are compared in Fig. 3(a). Experiments and computations reasonably agree with differences in the local maximum and minimum at the flag extreme position. However, comparison of tip trajectories with the data of Kim et al (2013) and Gilmanov et al. (2015) not only agree well but also resolve the two local deflection maxima (minima) that occur in the vicinity of maximum (minimum) flag deflection for $\beta = 0.1$, Fig 3(b).

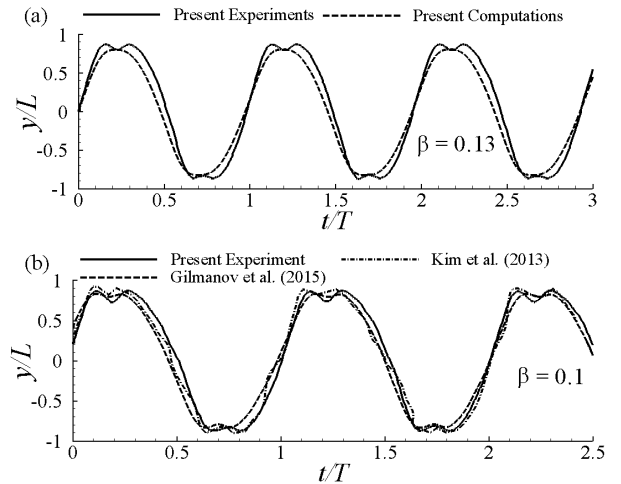


Figure: 3 Comparison of flag tip trajectories: (a) Present experiments and computations ($\beta = 0.13$) and (b) Comparison of present experiment with experiments of Kim et al. (2013) and computations of Gilmanov et al. (2015) for ($\beta = 0.1$).

For energy harvesting, one of the most important characteristics is its peak-to-peak amplitude (A/L) in the periodic flapping regime. Larger values of A/L , results in larger curvature and thus lead to high mean strain energy (Ryu et al. 2015). Measurements indicate that the maximum amplitude of the flag A/L is in the range of 1.7 to 1.8 and is insensitive to Reynolds number (Re). Peak-to-peak amplitude significantly changes with the dynamics of the system, i.e it increases as the flag changes from deflected mode to flapping mode and decreases from flapping to stable equilibrium mode, Fig. 4(a).

The flapping frequency of the flag for varying bending stiffness is compared with measurements of Kim et al. (2013) and is shown in Fig. 4(b). The flag exhibits maximum flapping frequency in the vicinity of Strouhal number (St) 0.16 for bending stiffness 0.21. Further, it is observed that the flapping frequency

increases for decreasing bending stiffness indicating that the flag changes from equilibrium mode to flapping mode. A decrease in flapping frequency is observed especially as the flag undergoes a change from periodic flapping to deflected or biased mode indicating cessation of flapping.

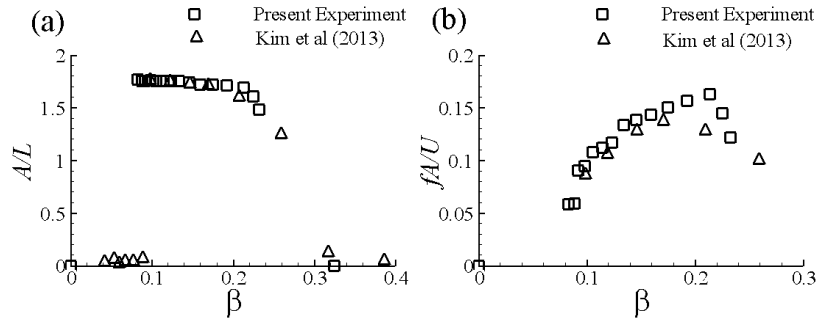


Figure 4: Variation of flapping amplitude and frequency of an inverted flag

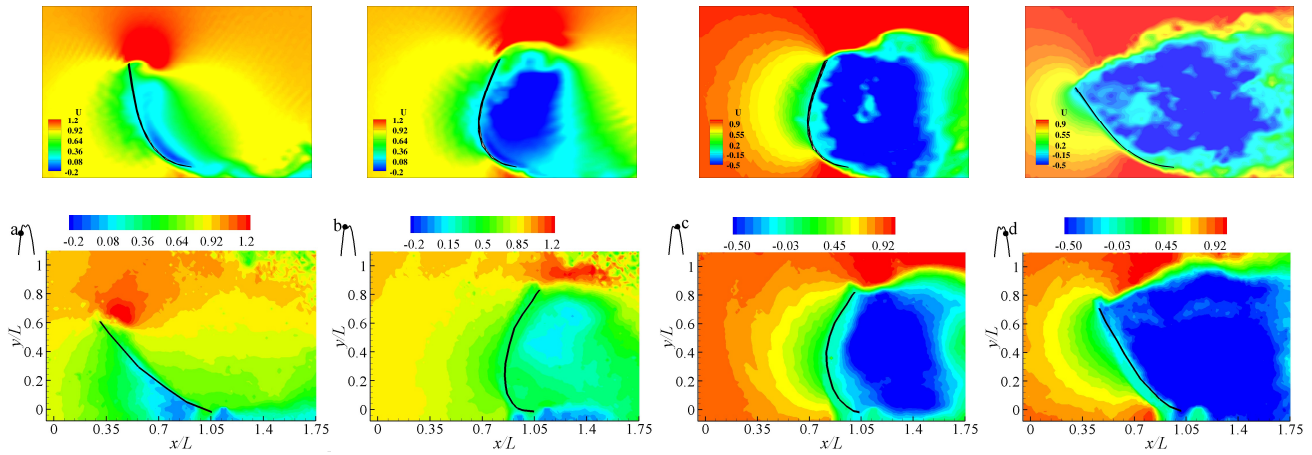


Fig. 5 Comparison of streamwise velocity contours for sequences of flag position in vicinity of maximum deflection: Top row instantaneous flow field from numerical simulations; bottom row phase averaged flow field from PIV measurements (solid black line indicates flag, a to d, $y/L = 0.6, 0.86, 0.88$ and 0.78 respectively). Note: velocity scale of a, b differs from c, d.

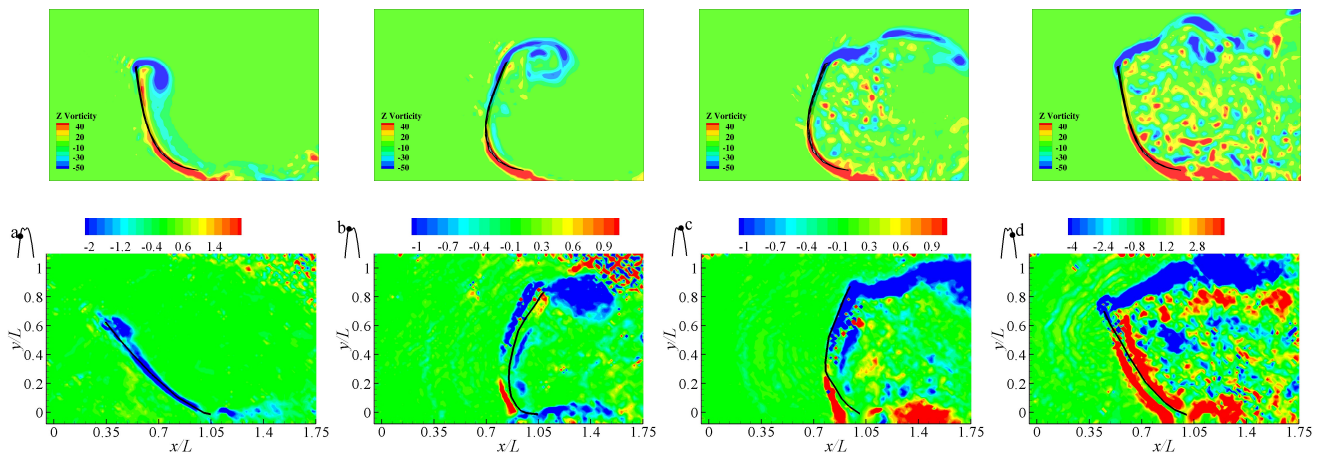


Fig. 6 Computational instantaneous contours of Z-vorticities (top row) and phase averaged experimental data (bottom row) for sequences of flag position in vicinity of maximum deflection. (solid black line indicates flag, a to d, $y/L = 0.6, 0.86, 0.88$ and 0.78 respectively)

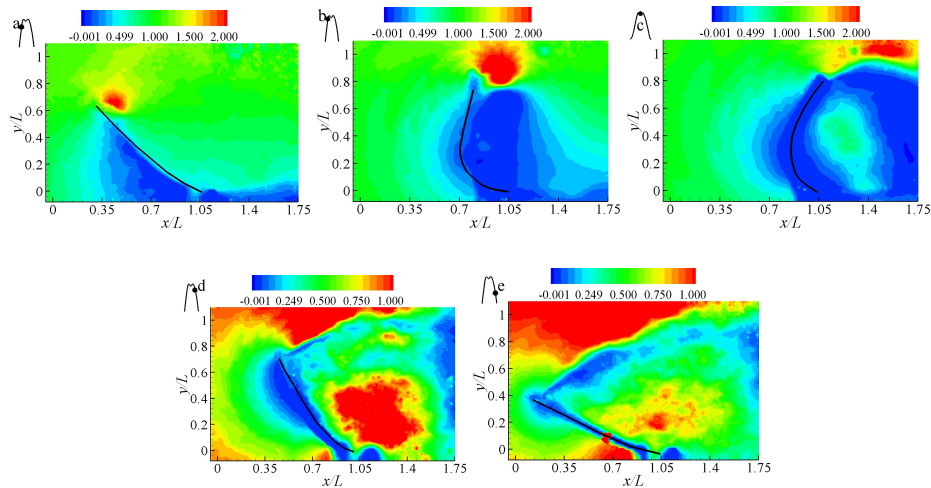


Figure: 7 Normalised phase averaged contours of Reynolds stress ($\langle u'v' \rangle$) for varying flag positions during forward and return phase of the flag. (a to e, $y/L = 0.6; 0.86; 0.88; 0.78$ and 0.36 respectively)

Flow dynamics related to large amplitude flapping

In this section, phase-averaged measurements based on the PIV images are presented. Fifty instantaneous image pairs are used for the averaging. Analyses has been carried out at specific locations during the forward and return legs of the flag motion.

Figure 5 indicates a comparison between the instantaneous velocity field obtained from numerical simulations (top row) and the phase averaged contours of the streamwise velocity ($\langle u \rangle$) from the experiments (bottom row). It should be noted that the phase averaged information was not collected during the computations, and hence the comparison between the experiments and predictions should be viewed as qualitative, and show good agreement. Further since the phase-averaging is only done with a limited number of data sets, some evidence of jitter in the phase-averaged measurements can be seen, particularly in the derived quantities such as vorticity.

The contours in Fig. 5 show that, as the flag moves upwards from position “a”, a vortex begins to form because of shear-layer instability and rollup (Fig. 6), leading to an unsteady flow separation behind the flag tip. As the flag moves to the position of maximum deflection, the separation at the leading-edge grows (“blue-colored” regions in position “b”), leading to vortex growth (a to b). At the peak position, the pressure difference across the flag are balanced by the structural forces, and as the vortex breakdown occurs, the pressure differences decrease leading the flag to retract from the maximum deflected position. Thus, a periodically varying pressure difference between the leading side and the trailing side of the flag is established, associated with the vortex shedding and breakdown cycles, and lead to the flag-oscillations. At the peak position of the flag i.e. at the location marked by “b”, the separated region and the leading-edge vortex are clear and distinct. As the flag recedes from the peak position, evidence of vortex breakdown occurs (Figs 6c and 6d), the separated region further increases and fluctuations begin to dissipate into free-stream as the flag retracts. The growth and breakdown of large-scale structures is clearly observed through the contours of vorticity (Fig.6).

The above noted discussion is consistent with the mechanisms of vortex-induced-vibration behind flexible bluff bodies where periodic vortex-shedding is observed. The formation of these

vortices results from the rollup of the unstable shear layers generated at the flow separation and this phenomenon induces an alternating pressure loading on the cylinder surface and a transverse force at frequency close to shedding frequency (Bearman 1984; Sarpkaya 1979; and Blevins 1977). Current observations, along with study of Sader et al. (2016) reveal that an inverted flag similarly exhibits periodic vortex shedding past the zero equilibrium position owing to leading-edge separation and vortex shedding. An inverted flag being an elastic bluff body experiences the periodic hydrodynamic force due vortex shedding which in turn can induce oscillations synchronized with vortex shedding, which is a primary characteristic of the VIV of an elastic bluff body.

The normalized phase averaged Reynolds stresses are shown in Fig. 7. During the forward motion of the flag at “a”, it is observed that as the flow undergoes separation at the leading edge, high values of the Reynolds stresses are found at the tip similar to that found in other applications involving separated flows (Samson and Sarkar 2015, Hain et al. 2009). This region of high shear, associated with the shear layer around the vortex, grows and moves upwards as the flag reaches its maximum deflected position. With the primary vortex breakdown, and the development of smaller eddies in the wake of the flag (Fig. 6c and 6d), high shear stresses are seen in the wake regions reflecting the turbulent interchange between the smaller scale eddies. High regions of shear are also seen in the outward regions as the retracting flag begins to reverse the flow leading to regions of counter-shear in the outer regions.

CONCLUDING REMARKS

An experimental and computational study is undertaken to understand the flow behavior of an inverted flag. PIV images were phase averaged with respect to the flag position. The measured data for the maximum deflection, and frequency agree well with the computations undertaken here and the published data in the literature. The images of the velocity field at different time instances agree qualitatively between the measurements and computations. The results indicate that the flag oscillations are controlled by the vortex-shedding behind the tip of the flag, its

growth and breakdown process. The behavior of the flow structures strongly influence the spatio-temporal distributions of the Reynolds stresses.

REFERENCES

- Alben, S., and Shelley, M., 2008, "Flapping States of a Flag in an Inviscid Fluid: Bistability and the Transition to Chaos". *Physical Review Letters* (100), 1-4.
- Allen, J. J., and Smits, A. J., 2001, "Energy Harvesting EEL", *J. Fluids Struct.* Vol. 15, pp. 1–12.
- Argentina, M., and Mahadevan, L., 2005, "Fluid-flow-induced Flutter of a Flag", *Proc. Natl Acad. Sci. USA* Vol. 102, pp. 1829–1834.
- Bearman, P. W., 1984, „Vortex Shedding from Oscillating Bluff Bodies“, *Annu. Rev. Fluid Mech.* 16, 195–222.
- Blevins, R. D. 1977. Fluid Elastic Whirling of Tube Rows and Tube Arrays. *Journal of Fluids Engineering* 99, 457-461.
- Connell, B. S. H., and Yue, D. K. P., 2007, "Flapping Dynamics of a Flag in a Uniform Stream", *J. Fluid Mech.*, Vol. 581, pp. 33–67.
- Eloy, C., Souilliez, C., and Schouveiler, L., 2007, "Flutter of a Rectangular Plate", *J. Fluids Struct.*, Vol. 23, pp. 904–919.
- Eloy, C., Lagrange, R., Souilliez, C., and Schouveiler, L., 2008, "Aeroelastic Instability of Cantilevered Flexible Plates in Uniform Flow", *J. Fluid Mech.*, Vol. 611, pp. 97–106.
- Gilmanov, A., Le, T., and Sotiropoulos, F., 2015. "A Numerical Approach for Simulating Fluid Structure Interaction of Flexible Thin Shells Undergoing Arbitrarily Large Deformations in Complex Domains". *J. Comput. Phys.*, 300, pp. 814–843.
- Hain, R., Kahler, C. J., and Radespiel, R., 2009, "Dynamics of Laminar Separation Bubbles at Low-Reynolds-Number Aerofoils", *J. Fluid Mech.*, Vol. 630, pp. 129–153.
- Huang, L., 1995, "Flutter of Cantilevered Plates in Axial Flow", *J. Fluids Struct.*, Vol. 9, pp.127–147.
- Huang, W.X., and Sung, H. J., 2010, "Three-dimensional Simulation of a Flapping Flag in a Uniform Flow", *J. Fluid Mech.*, Vol. 653, pp. 301–336.
- Huang, I., Rominger, J. and Nepf, H. 2011 The Motion of Kelp Blades and Surface Renewal Model. *Limnol. Oceanogr.* 56 (4), 1453–1462.
- Jaiman, R. K., Loth, E. and Dutton, J. C. 2004 Simulations of Normal Shock-wave/Boundary-layer Interaction Control Using Mesoflaps. *AIAA J. Propul. Power* 20, 344–352.
- Kang, S, Lightbody, A., Hill, G, Sotiropoulos, F, High-resolution Numerical Simulation of Turbulence in Natural Water ways, *Adv. Water Resour.* 34 (2011) 98–113.
- Kim, D., Cosse, J., Cerdeira, C. H., and Gharib, M., 2013, "Flapping Dynamics of an Inverted Flag", *J. Fluid Mech.*, 736.
- Lucey, A. D., 1998, "The Excitation of Waves on a Flexible Panel in a Uniform Flow". *Phil. Trans. R. Soc. Lond. A* 356, 2999–3039.
- Michelin, S., Llewellyn Smith, S. G., and Glover, B. J., 2008, "Vortex Shedding Model of a Flapping Flag", *J. Fluid Mech.*, Vol. 617, pp. 1–10.
- Michelin, S. and Doare, O., 2013, "Energy Harvesting Efficiency of Piezoelectric Fags in Axial Flows", *J. Fluid Mech.* Vol. 714, pp. 489–504.
- Rinaldi, S. & Paidoussis, M. P., 2012, "Theory and Experiments on the Dynamics of a Free-clamped Cylinder in Confined Axial Air-flow", *J. Fluids Struct.* Vol. 28, pp. 167–179.
- Samson, A., and Sarkar, S., 2015, "Effects of Free-Stream Turbulence on Transition of a Separated Boundary Layer Over the Leading-Edge of a Constant Thickness Airfoil. *ASME. J. Fluids Eng.* Vol. 138(2), 021202-021202-19.”,
- Sarpkaya T., 1979, "Vortex-induced Oscillations", *ASME J. Appl. Mech.* Vol. 46, pp. 241–58
- Stolarski, H., Gilmanov, A., and Sotiropoulos, F., 2013, "Non-linear Rotation-free 3-node shell Finite-element Formulation", *International Journal for Numerical Methods in Engineering*; Vol. 95, pp.740-770.
- Sader, J., Cossé, J., Kim, D., Fan, B., and Gharib, M., 2016, "Large-amplitude Flapping of an Inverted Fag in a Uniform Steady Flow – a Vortex-induced Vibration", *J. Fluid Mech.*, Vol. 793, pp. 524-555.
- Shelley, M. J., and Zhang, J. 2011, "Flapping and Bending Bodies Interacting with Fluid Flows", *Annu. Rev. Fluid Mech.*, Vol. 43, pp. 449–465.
- Tang, L., Paidoussis, M. P. and Jiang, J., 2009, "Cantilevered Flexible Plates in Axial Flow: Energy Transfer and the Concept of Flutter-mill", *J. Sound Vib.*, Vol. 326, pp. 263–276.
- Tang, C., Liu, N.-S. and Lu, X.-Y. 2015, "Dynamics of an Inverted Flexible Plate in a Uniform Fow", *Phys. Fluids*, Vol. 27, 073601
- Watanabe, Y., Suzuki, S., Sugihara, M., and Sueoka, Y., 2002a, "An experimental study of paper flutter", *J. Fluids Struct.*, Vol. 16, pp. 529–542.
- Watanabe, Y., Suzuki, S., Sugihara, M. and Sueoka, Y. 2002b "An experimental study of paper flutter", *J. Fluids Struct.* Vol. 16, 529–542.
- Zhu, L., and Peskin, C. S., 2002, "Simulation of a Flapping Flexible Filament in a Flowing Soap Film by the Immersed Boundary Method", *J. Comput. Phys.*, Vol. 179, pp. 452–468.